Journal of Alloys and Compounds 509 (2011) L69–L73

Contents lists available at ScienceDirect

Journal of Alloys and Compounds

journal homepage: www.elsevier.com/locate/jallcom

Letter

Fabrication of $V_3O_7{\cdot}H_2O$@C core-shell nanostructured composites and the effect of $V_3O_7{\cdot}H_2O$ and $V_3O_7{\cdot}H_2O$@C on decomposition of ammonium perchlorate

Yifu Zhang [a], Xinghai Liu [b,*], Dongzhi Chen [a], Lei Yu [a], Jiaorong Nie [c], Shengping Yi [a], Houbin Li [b], Chi Huang [a,*]

[a] Engineering Research Center of Organosilicon Compound and Material, Ministry of Education of China, College of Chemistry and Molecular Sciences, Wuhan University, Wuhan 430072, PR China
[b] School of Printing and Packaging, Wuhan University, Wuhan 430079, PR China
[c] Jianghe Chemical Factory of CSSG, Yuan'an 444200, PR China

ARTICLE INFO

Article history:
Received 14 August 2010
Received in revised form 12 October 2010
Accepted 28 October 2010
Available online 4 November 2010

Keywords:
$V_3O_7{\cdot}H_2O$@C
Core-shell structure
Composite materials
Thermal analysis

ABSTRACT

$V_3O_7{\cdot}H_2O$@C core-shell materials have been synthesized using $V_3O_7{\cdot}H_2O$ nanobelts as the cores and glucose as the source of carbon via an environmental hydrothermal method. The as-obtained $V_3O_7{\cdot}H_2O$@C core-shell materials were characterized by X-ray powder diffraction (XRD), transmission electron microscopy (TEM), elemental analysis (EA), Fourier transform infrared spectroscopy (FT-IR) and Raman spectrum. The influences of the reaction temperature, concentration of glucose and reaction time on the morphologies of the samples were respectively discussed in detail. The possible formation mechanism of $V_3O_7{\cdot}H_2O$@C was proposed according to our experimental results. Furthermore, the effect of $V_3O_7{\cdot}H_2O$ and $V_3O_7{\cdot}H_2O$@C on the thermal decomposition of ammonium perchlorate (AP) were investigated by thermal gravimetric analyzer (TG) and differential thermal analysis (DTA). The thermal decomposition temperatures of AP in the presence of $V_3O_7{\cdot}H_2O$ and $V_3O_7{\cdot}H_2O$@C were reduced by 70 and 89 °C, respectively, which indicates that $V_3O_7{\cdot}H_2O$@C core-shell composites have higher activity than $V_3O_7{\cdot}H_2O$.

1. Introduction

As is well known, ammonium perchlorate (AP) is the most common oxidizing agents which have been used in various solid propellants. The thermal decomposition properties influence the combustion behavior of the solid propellants. In the past few decades, thermal decomposition of AP has been extensively investigated by taking advantages of the catalytic activities of many transition metal oxides and their related composites (e.g. CuO, Fe_2O_3, Mn_2O_3, Cr_2O_3, Ni@CNTs, Co/MFe_2O_4 (M = Fe, Mn)) [1–4]. However, to find new catalysts which applied in the thermal decomposition of AP is still a great challenge for material scientists who are engaging in the field of catalyst. To our best knowledge, vanadium oxides and their derivatives used as the catalysts on the thermal decomposition of AP have not been reported.

Vanadium oxides and their related compounds have been extensively studied in recent years, because of their layered structure, novel chemical and physical properties, which make them possess a lot of broad applications, such as, cathode materials for reversible lithium batteries, catalysts, gas sensors, intelligent thermochromic windows, optical switching devices, optical or electrical modulators and so on [5–11]. As a new class of vanadium oxides, vanadium oxide hydrate ($V_3O_7{\cdot}H_2O$) has attracted more and more attention and a lot of work has been devoted to study its magnetic, electrochemical and catalytic properties recently [12–15]. However, few reports have been done to study the effect of $V_3O_7{\cdot}H_2O$ in thermal decomposition of AP.

Recently, amorphous carbon is one of the most important materials in many applications owing to its chemical inertness, biocompatibility, high wear resistance, and high thermal conductivity [16,17]. Thus, the ideal coating carbon on the surface of $V_3O_7{\cdot}H_2O$ nanobelts can be used to explore a novel research field based on surface modification to improve the inherent properties of $V_3O_7{\cdot}H_2O$ nanobelts. Although some reports have been studied the metal oxides coated with amorphous carbon [18,19], the $V_3O_7{\cdot}H_2O$@C core-shell structure has not been investigated. So, in this study, we will introduce the amorphous carbon to coat on the surface of $V_3O_7{\cdot}H_2O$ nanobelts to improve their catalytic activity. Fortunately, this novel core-shell material has good performance in decomposition of AP.

In this communication, we have successfully fabricated the $V_3O_7{\cdot}H_2O$@C core-shell materials using $V_3O_7{\cdot}H_2O$ nanobelts as the cores and glucose as the source of carbon via an environmental hydrothermal method. And then, the effect of $V_3O_7{\cdot}H_2O$ and

* Corresponding authors. Tel.: +86 27 68752701; fax: +86 27 68754067.
E-mail addresses: liuxh@whu.edu.cn (X. Liu), chihuang@whu.edu.cn (C. Huang).

0925-8388/$ – see front matter.
doi:10.1016/j.jallcom.2010.10.154

$V_3O_7{\cdot}H_2O$@C on the thermal decomposition of AP was investigated by DTA and the results indicated that $V_3O_7{\cdot}H_2O$@C core-shell composites have higher catalytic activity than that of $V_3O_7{\cdot}H_2O$, achieving the aim of improving the catalytic activity of $V_3O_7{\cdot}H_2O$.

2. Experimental

2.1. Materials

Vanadium pentoxide (V_2O_5), ethanol, D-(+)-glucose and ammonium perchlorate (AP) were purchased from Sinopharm Chemical Reagent Co., Ltd. and used without any further purification.

2.2. Synthesis of $V_3O_7{\cdot}H_2O$ nanobelts

The synthesis of $V_3O_7{\cdot}H_2O$ nanobelts was based on our previous report [20]. In a typical synthesis, 9.00 g of V_2O_5 powder was dispersed into 100 mL of ethanol, and then 300 mL of deionized water was added into the above solution with magnetic stirring. The mixed solution was transferred into a 600 mL stainless steel autoclave after the solution became suspension. The autoclave was sealed and maintained at 180 °C for 24 h and then cooled to room temperature naturally. The products were filtered off, washed with distilled water and absolute ethanol several times to remove any possible residue, and dried in vacuum at 75 °C for future application. The morphologies of the starting materials were represented in Fig. S1 (Supplementary data).

2.3. Synthesis of $V_3O_7{\cdot}H_2O$@C core-shell composites

In a typical procedure, 0.4 g of the as-obtained $V_3O_7{\cdot}H_2O$ nanobelts were dispersed into the glucose solution (a certain amount of glucose (1.0, 2.0, 3.0 or 4.0 g) and 45 mL of distilled water) in a 100 mL beaker under ultrasonic for 20 min, and then the mixture was stirred vigorously for 1 h by magnetic stirrer. After the solution became suspension, they were transferred into a 60 mL stainless steel autoclave, which was sealed and maintained at different temperatures (140, 160, 180 or 200 °C) for the designated time (1, 1.5, 3, 4 or 6 h). After cooling to room temperature naturally, the products were filtered off, washed with distilled water and absolute ethanol several times, and dried in vacuum at 75 °C for further characterization and application.

2.4. Characterization

The morphologies of the products were observed by transmission electron microscopy (TEM, JEM-100CXII). X-ray powder diffraction (XRD) was carried out on D8 X-ray diffractometer equipment with Cu *Kα* radiation, λ = 1.54060 Å. Data was collected between 8° and 80° with a scan speed of 4°/min. The Raman spectrum was taken on a RM-1000 spectrometer (Confocal Raman Microspectroscopy) from 800 to 2000 cm^{-1} with an argon-ion laser at an excitation wavelength of 514.5 nm. The elemental analysis of the samples was carried out using a Vario EL III equipment (Germany) with a TCD detector to analyze the element of C, H, N and S. Fourier transform infrared spectroscopy (FT-IR) pattern of the solid samples was measured using KBr pellet technique (About 1 wt% of the samples and 99 wt% of KBr were mixed homogeneously, and then the mixture was pressed to a pellet) and recorded on a Nicolet 60-SXB spectrometer from 4000 to 400 cm^{-1} with a resolution of 4 cm^{-1}. Thermo-gravimetric analysis and differential thermal analysis (TG/DTA) measurements were performed on Diamond TG-DTA 6300. Measurements were performed on ~10 mg of precursor powder, in an Al_2O_3 crucible, over the range 50–500 °C, at a heating rate of 10 °C/min, and under nitrogen flux (~80 mL/min). Before the measurements, AP and the as-obtained samples were mixed at a mass ratio of 98:2 and ground to make them dispersed homogeneously to prepare the target samples for thermal decomposition analyses.

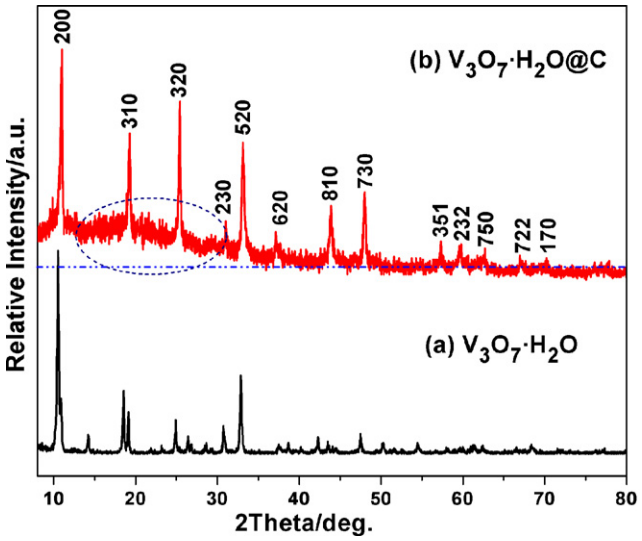

Fig. 1. XRD patterns of the as-obtained products.

3. Results and discussion

3.1. Characterization of the resulting products

The phase and composition of the as-obtained products were investigated by XRD test, as depicted in Fig. 1. All the peaks from Fig. 1a can be readily indexed to the orthorhombic crystalline phase (space group: *Pnam*) of $V_3O_7{\cdot}H_2O$ in agreement with the literature values (JCPDS No. 85-2401) [21]. After the coating process, all the peaks from Fig. 1b can be assigned to the phase of $V_3O_7{\cdot}H_2O$ (JCPDS No. 85-2401). No characteristic peaks due to the impurities of other vanadium oxides were detected, which indicates that the products obtained by the present synthetic route consist of a pure orthorhombic phase. Naturally, some peaks of $V_3O_7{\cdot}H_2O$ are not detected compared Fig. 1a with Fig. 1b, which indicates that some materials are probably coated on the surface of $V_3O_7{\cdot}H_2O$. In addition, we can also see a broadened peak ranging from 15° to 30° compared with base line, which is attributed to amorphous carbon [18,22]. These results reveal that $V_3O_7{\cdot}H_2O$ are encapsulated into the carbon and $V_3O_7{\cdot}H_2O$@C core-shell composites are successfully fabricated.

In order to get a clear insight into the core-shell structure of the resulting products, the corresponding TEM measurement was

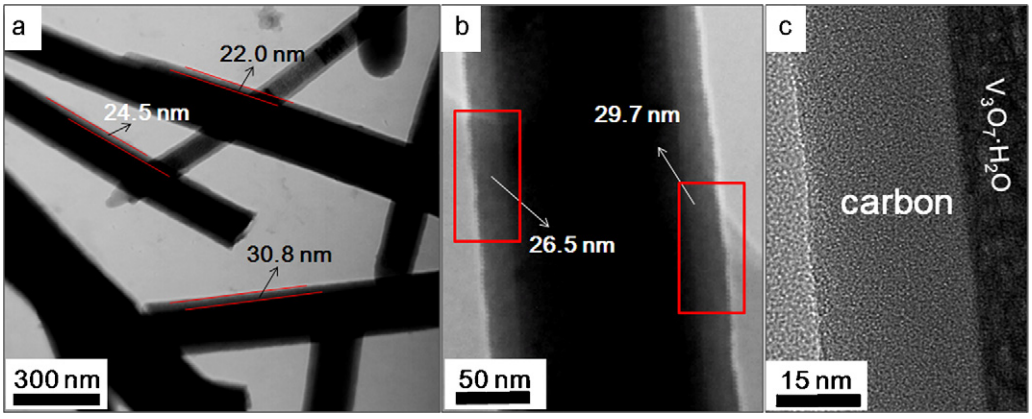

Fig. 2. TEM images of the resulting products.

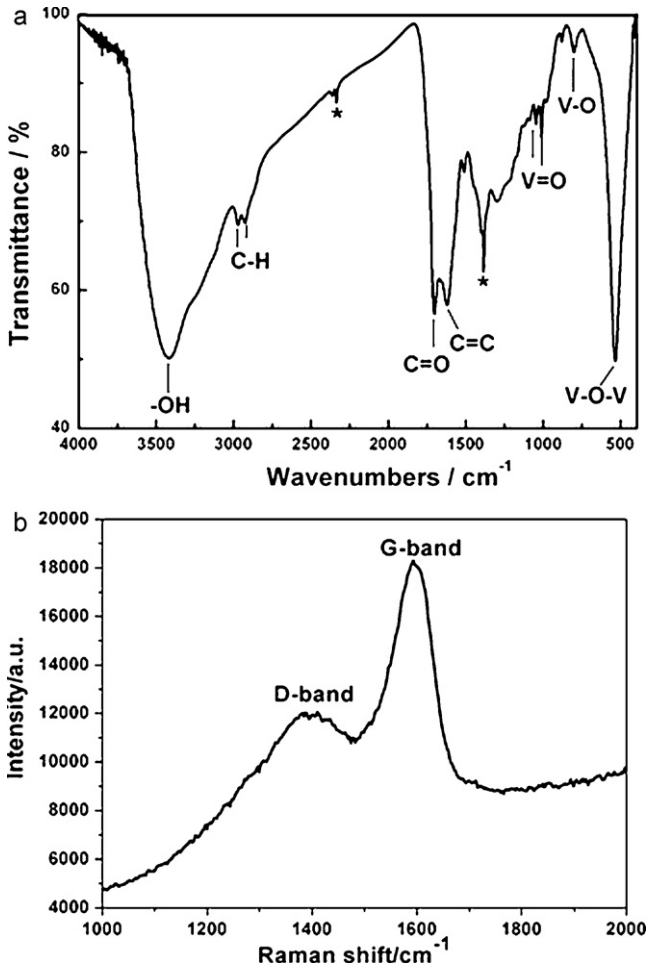

Fig. 3. (a) FT-IR spectrum of $V_3O_7{\cdot}H_2O$@C and (b) Raman spectrum of $V_3O_7{\cdot}H_2O$@C.

carried out, as shown in Fig. 2. After coating process, the samples consist of well-defined nanoblets with length up to several micrometers, and the contrast grade between core and shell could even be observed, indicating that each $V_3O_7{\cdot}H_2O$ core is encapsulated into carbon. The average thickness of the shells is 25.8 nm collected from all TEM images. The higher magnification TEM image (Fig. 2c) further shows that the as-obtained samples have core-shell structures with $V_3O_7{\cdot}H_2O$ cores and carbon shells.

Further information about the composition of the as-obtained core-shell composites was collected from the EA, FT-IR and Raman measurements. The result of EA shows that the $V_3O_7{\cdot}H_2O$@C composite at least contains 28.15 wt% of C and 4.22 wt% of H, implying that it probably contains some organic functional groups, which is further confirmed by FT-IR (Fig. 3a). According to the FT-IR spectrum, we can find that C=O (1707 cm^{-1}) and C=C (1618 cm^{-1}) groups exist in $V_3O_7{\cdot}H_2O$@C core-shell composite, which also supports the concept of aromatization of glucose during hydrothermal treatment [17]. The peaks at 3450 cm^{-1} and 2950–2850 cm^{-1} are the characteristic O–H and C–H stretches, respectively, implying the existence of large numbers of residual O–H and C–H groups after the carbonized process. The peaks at 1020 cm^{-1}, 1000 cm^{-1}, 780 cm^{-1} and 534 cm^{-1} are attributed to the characteristic of V–O vibration band. The bands at 1020 cm^{-1} and 1000 cm^{-1} correspond to the symmetric stretching of the $\nu_s(V^{5+}{=}O)$ and $\nu_s(V^{4+}{=}O)$ bonds [23], respectively. The signals at 780 cm^{-1} and 534 cm^{-1} can be attributed to the vibrational band characteristic of V–O–V [12,24]. In addition, the absorptions at 2336 cm^{-1} and 1388 cm^{-1} are due to carbon dioxide and nitrate, respectively, adsorbed on the KBr and can be disregarded [25]. Fig. 3b represents a typical Raman spectrum of the $V_3O_7{\cdot}H_2O$@C core-shell composite, which exhibits two main peaks. The peaks centered at 1388 cm^{-1} and 1596 cm^{-1} are corresponding to the in-plane vibration of disordered amorphous carbon (D band) and crystalline graphic carbon (G band), respectively, which are the same as those of amorphous carbon [19,26]. The intensity ratio of the G- and D-bands was $I_G/I_D = 1.50$ for the resulting product. The relatively high intensity of the D-peak further proves that the coating comprises disordered carbon. Therefore, the Raman spectrum further confirms that the carbon coating on the surface of $V_3O_7{\cdot}H_2O$ is disordered, in agreement with XRD pattern observation. All above analyses (XRD, TEM, EA, FT-IR and Raman) reveal that the as-obtained samples are $V_3O_7{\cdot}H_2O$@C core-shell composites and the shells consist of amorphous carbon with aromatic structure containing lots of active function groups such as C=C and C=O, which will facilitate the linkage of catalytic species or biomolecules to the surface in potential applications.

3.2. Some parameters controlled the fabrication of $V_3O_7{\cdot}H_2O$@C core-shell structures

The thicknesses of the carbon coating on the surface of $V_3O_7{\cdot}H_2O$ nanoblets were greatly influenced by the reaction temperature, concentration of glucose and reaction time. When the reaction temperature was below 140 °C keeping other parameters unchanged, the carbon shells could not be formed, as shown in Fig. S2a (Supplementary data). We can see that $V_3O_7{\cdot}H_2O$@C could be obtained at 160 °C (Fig. S2b). When the temperature was raised to 200 °C, the carbon shells ranging from 40 to 140 nm were coated on the surface of $V_3O_7{\cdot}H_2O$, as shown in Fig. S2c and d. The composites were aggregative and the thickness of the carbon was not well-distributed (a large distribution). The thickness of the shell was obviously changed with the glucose as the changeable parameter. With 1.0 g of glucose used in the experiment, the samples with the mixed phases (VO_2 is the main phase) were obtained, which was determined by XRD (Fig. S3). The reason for these can be that the glucose acts as the reducing reagent when the concentration of glucose is low. The TEM image (Fig. S4a) revealed that the short and broken belts were obtained. However, with the concentration of glucose increased, the thickness of the carbon shell was rapidly thickened. For example, the thicknesses were respectively about 60 and 80 nm on average when 3 g and 4 g of glucose were used in our experiments (Fig. S4b and c), which is much thicker than the products obtained using 2 g of glucose (26 nm). The reaction time has also influenced the thickness of the samples. When the reaction time was less than 1.5 h, only $V_3O_7{\cdot}H_2O$ was obtained. For example, Fig. 4a represents the sample obtained at 1 h and we cannot see the core-shell structure. However, with the time increased to 1.5 h or more, the resulting products with core-shell structure were prepared, as shown in Fig. 4b–d. The thickness of carbon shell became thick with the reaction time prolonged. As the time increased from 1.5 to 3, 4 and 6 h, the average thickness grew from 19.6 (Fig. 4b) to 25.8 (Fig. 2), 31.4 (Fig. 4c), and 31.9 nm (Fig. 4d). However, the thickness of the carbon shell had little changes after 4 h, which might be due to that the carbonization of the glucose was finished.

3.3. Formation mechanism

According to our synthetic route, this process can be regarded as the post-synthesis technology. It has been reported that the surface of cores containing some active function groups (e.g. hydroxyl group) will facilitate the coating process [18]. As is well known, $V_3O_7{\cdot}H_2O$ nanobelts have been prepared using V_2O_5 as the source of vanadium in the mixed solution (water and ethanol), whose surface is probably accompanied with some hydroxyl groups, which is proved by FT-IR, as shown in Fig. S5 and in agreement with

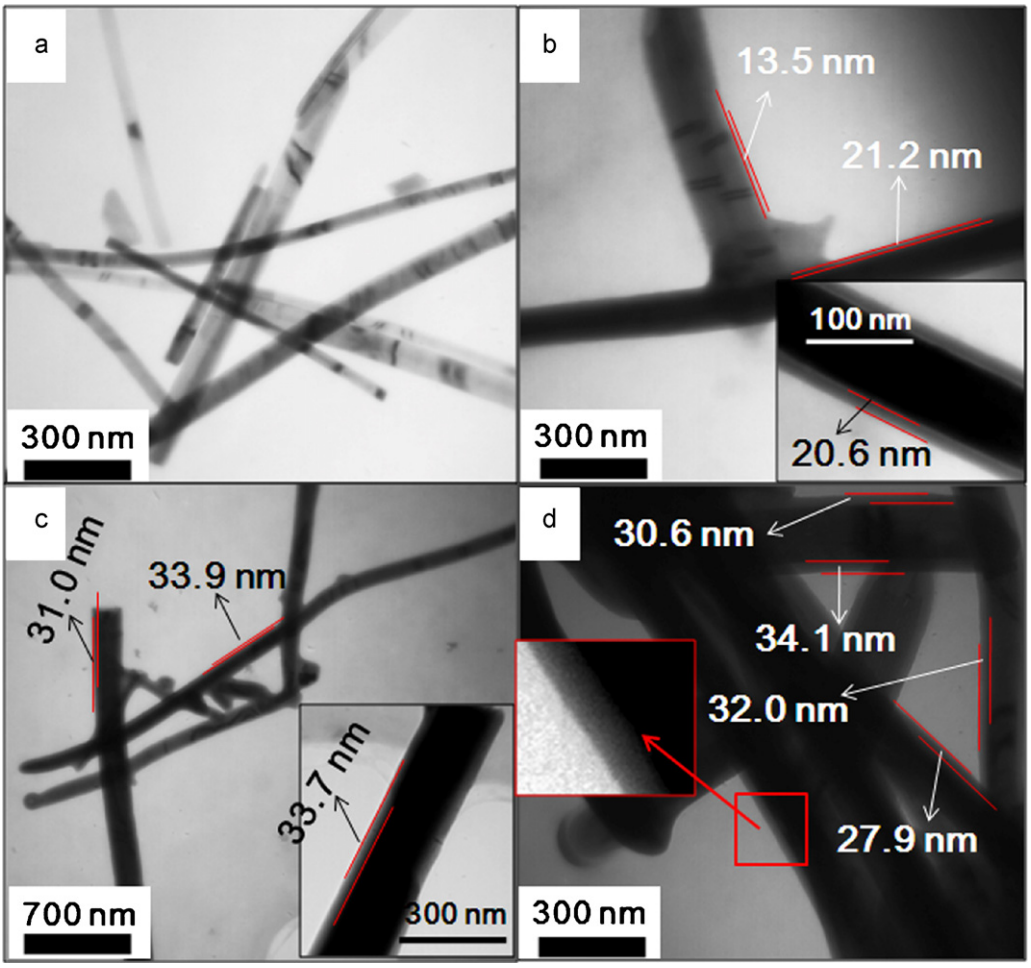

Fig. 4. TEM images of the resulting products obtained with different time: (a) 1 h, (b) 1.5 h, (c) 4 h, (d) 6 h. An enlarged image was respectively inserted in (b), (c) and (d).

our previous report [20], too. The colloid carbon spheres were synthesized using only glucose solution under the hydrothermal condition reported by Sun [17]. First, the glucose is dehydrated to form oligosaccharides. Then, when the solution reached a critical supersaturation, the oligosaccharides are involved in intermolecular dehydration, cross-linking and carbonization. Finally, the colloid carbon spheres are formed. Based on all the results discussed above, in this communication, we have proposed a "carbonization adsorption growth" (CAG) mechanism to explain the formation of $V_3O_7{\cdot}H_2O$@C, which mainly contain three steps. Fig. 5 represents the schematic illustration of the formation mechanism of $V_3O_7{\cdot}H_2O$@C core-shell structure. First, because of their hydrophilic nature, $V_3O_7{\cdot}H_2O$ can be dispersed into aqueous solution of glucose to form a stable suspension, which was supported by Fig. S6. So the glucose molecules can be fully in touch with $V_3O_7{\cdot}H_2O$. Second, the glucose is proceeded intermolecular dehydration, polymerization and carbonization to form small carbon spheres, which can be adsorbed on the surface of $V_3O_7{\cdot}H_2O$ nanoblets due to their surface containing some hydroxyl groups or their large surface area or their high surface energy. Last, the glucose is continuing carbonization to form the amorphous carbon which is loaded on the surface of $V_3O_7{\cdot}H_2O$ nanoblets, resulting in that the carbon shells of $V_3O_7{\cdot}H_2O$@C core-shell materials become thicker and thicker with the reaction time prolonged. This can be explained by that the average thickness of the shell is from 19.6 (Fig. 4b) to 25.8 (Fig. 2), 31.4 (Fig. 4c), and 31.9 nm (Fig. 4d) as the time increased from 1.5 to 3, 4 and 6 h. Furthermore, the similar mechanism has been successfully explained the formation of Fe_3O_4@C [22] and Ag@C [27].

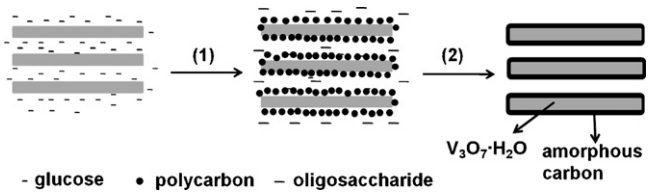

Fig. 5. Schematic illustration of the formation mechanism of $V_3O_7{\cdot}H_2O$@C core-shell structure.

3.4. The influence on the thermal decomposition of AP

The TG and DTA curves of pure AP, AP in the presence of $V_3O_7{\cdot}H_2O$ and AP in the presence of $V_3O_7{\cdot}H_2O$@C core-shell materials were shown in Fig. 6A and B. It could be observed from Fig. 6A that the addition of $V_3O_7{\cdot}H_2O$ or $V_3O_7{\cdot}H_2O$@C in AP led to a significant reduction of the ending decomposition temperature of AP. There is no weight loss at the endothermic peak (246 °C), which is due to the transition from orthorhombic to cubic AP [28] and is not influenced by the additive. The exothermic peaks at 317 °C and 453 °C in Fig. 6Ba are assigned to the partial decomposition of AP to form some intermediate products such as NH_3 and $HClO_4$ and then complete decomposition to volatile products [29], respectively. This progress can be also verified by TG (Fig. 6A) and TG-FTIR (this detail information is represented in Fig. S7, supplementary data).

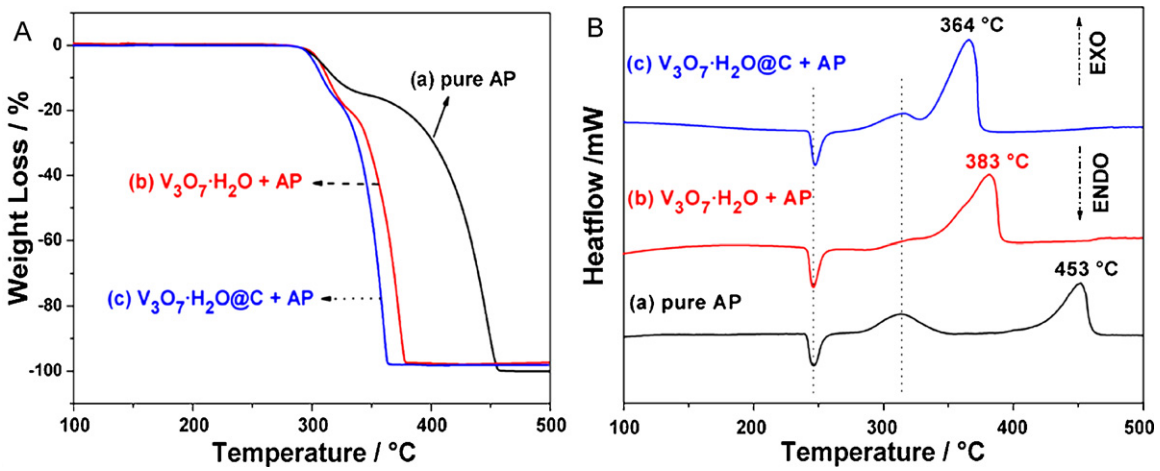

Fig. 6. TG and DTA curves for: (a) pure AP, (b) $V_3O_7·H_2O$ and AP, (c) $V_3O_7·H_2O$@C and AP.

Obvious changes can be observed in Fig. 6Bb and c. With 2 wt% of $V_3O_7·H_2O$ or $V_3O_7·H_2O$@C added, the thermal decomposition temperature of AP was lowered by 70 and 89 °C, respectively. So we can conclude that both $V_3O_7·H_2O$ and $V_3O_7·H_2O$@C have high catalytic activity towards the thermal decomposition of AP, which may be used as the promising catalysts in the future. However, it is obvious that $V_3O_7·H_2O$@C core-shell composites have higher catalytic activity than $V_3O_7·H_2O$, which is corresponding with the suggested results discussed above. According to the traditional electron-transfer theory [28], we presume that the possible mechanism of the effect of $V_3O_7·H_2O$@C on the thermal decomposition of AP are as follows. On one hand, the presence of partially filled 3d orbit in vanadium atom provides help in electro-transfer process. Positive hole in vanadium atom can accept electrons from AP ion and its intermediate products, by which the thermal decomposition of AP is accelerated. On the other hand, the amorphous carbon containing aromatic structure with lots of active groups (such as C=C, C=O) verified by FT-IR are helpful to electron transfer and heat conduction, which also can promote the thermal decomposition of AP.

4. Conclusion

In conclusion, $V_3O_7·H_2O$@C core-shell structured materials have been synthesized using $V_3O_7·H_2O$ nanobelts as the cores and glucose as the source of carbon via an environmental hydrothermal method. The thickness of amorphous carbon with aromatic structure containing lots of organic function groups (such as C=C, C=O) is 25.8 nm on average. It was found that the reaction temperature, concentration of glucose and reaction time had significant influences on the phases and morphologies of the resulting products. We proposed the "carbonization adsorption growth" (CAG) mechanism to explain the formation of $V_3O_7·H_2O$@C core-shell structured materials. Furthermore, the results of DTA curves illustrate that the decomposition temperature of AP in the presence of $V_3O_7·H_2O$ and $V_3O_7·H_2O$@C was reduced by 70 and 89 °C, respectively, which indicated that $V_3O_7·H_2O$@C core-shell composites have higher catalytic activity than $V_3O_7·H_2O$.

Acknowledgements

This research work was partially supported by National Science Fund for Fostering Talents in Basic Science (J0730426), Natural Science Foundation of Hubei Province (2005ABA034), Key Laboratory of Catalysis and Materials Science of Hubei Province (CHCL06003) and Students' Scientific Research Program of Wuhan University (2007138). We thank Mr Shaobo Mo, Mr Weibing Wu and Mrs Ling Hu concerning the help of the TEM, FT-IR, TG and DTA.

Appendix A. Supplementary data

Supplementary data associated with this article can be found, in the online version, at doi:10.1016/j.jallcom.2010.10.154.

References

[1] L.J. Chen, L.P. Li, G.S. Li, J. Alloys Compd. 464 (2008) 532–536.
[2] I.P.S. Kapoor, P. Srivastava, G. Singh, Propell. Explos. Pyrotech. 34 (2009) 351–356.
[3] X.J. Zhang, W. Jiang, D. Song, J.X. Liu, F.S. Li, Mater. Lett. 62 (2008) 2343–2346.
[4] S. Peng, J. Xie, S.H. Sun, J. Solid State Chem. 181 (2008) 1560–1564.
[5] E. Strelcov, Y. Lilach, A. Kolmakov, Nano Lett. 9 (2009) 2322–2326.
[6] S.B. Ni, X.H. Wang, G. Zhou, F. Yang, J.M. Wang, D.Y. He, J. Alloys Compd. 491 (2010) 378–381.
[7] I.P. Parkin, T.D. Manning, J. Chem. Educ. 83 (2006) 393–400.
[8] Y. Wang, G. Cao, Chem. Mater. 18 (2006) 2787–2804.
[9] H.M. Zeng, Y. Zhao, Y.J. Hao, Q.Y. Lai, J.H. Huang, X.Y. Ji, J. Alloys Compd. 477 (2009) 800–804.
[10] S. Myung, M. Lee, G.T. Kim, J.S. Ha, S. Hong, Adv. Mater. 17 (2005) 2361–2364.
[11] E. Filipek, G. Dabrowska, M. Piz, J. Alloys Compd. 490 (2010) 93–97.
[12] S. Shi, M. Cao, X. He, H. Xie, Cryst. Growth Des. 7 (2007) 1893–1897.
[13] H. Qiao, X. Zhu, Z. Zheng, L. Liu, L. Zhang, Electrochem. Commun. 8 (2006) 21–26.
[14] G.S. Zakharova, V.L. Volkov, C. Täschner, I. Hellmann, A. Leonhardt, R. Klingeler, B. Büchner, Solid State Commun. 149 (2009) 814–817.
[15] F. Dong, S. Heinbuch, Y. Xie, J.J. Rocca, E.R. Bernstein, Z.-C. Wang, K. Deng, S.-G. He, J. Am. Chem. Soc. 130 (2008) 1932–1943.
[16] H.W. Ra, D.H. Choi, S.H. Kim, Y.H. Im, J. Phys. Chem. C 113 (2009) 3512–3516.
[17] X. Sun, Y. Li, Angew. Chem. Int. Ed. 43 (2004) 597–601.
[18] X.M. Sun, J.F. Liu, Y.D. Li, Chem. Mater. 18 (2006) 3486–3494.
[19] A. Odani, V.G. Pol, S.V. Pol, M. Koltypin, A. Gedanken, D. Aurbach, Adv. Mater. 18 (2006) 1431–1436.
[20] Y. Zhang, X. Liu, G. Xie, L. Yu, S. Yi, M. Hu, C. Huang, Mater. Sci. Eng. B 175 (2010) 164–171.
[21] Y. Oka, T. Yao, N. Yamamoto, J. Solid State Chem. 89 (1990) 372–377.
[22] S.H. Xuan, L.Y. Hao, W.Q. Jiang, X.L. Gong, Y. Hu, Z.Y. Chen, Nanotechnology 18 (2007) 1–6.
[23] T.R. Gilson, O.F. Bizri, N. Cheetham, J. Chem. Soc., Dalton Trans. (1973) 291–294.
[24] J.C. Valmalette, J.R. Gavarri, Mater. Sci. Eng. B 54 (1998) 168–173.
[25] T.G. Ros, A.J. van Dillen, J.W. Geus, D.C. Koningsberger, Chem. Eur. J. 8 (2002) 1151–1162.
[26] A. Ilie, C. Durkan, W.I. Milne, M.E. Welland, Phys. Rev. B 66 (2002), 045412/045411–045412/045413.
[27] X.M. Sun, Y.D. Li, Langmuir 21 (2005) 6019–6024.
[28] V.V. Boldyrev, Thermochim. Acta 443 (2006) 1–36.
[29] X.Q. Shi, X.H. Jiang, L.D. Lu, X.J. Yang, X. Wang, Mater. Lett. 62 (2008) 1238–1241.